Majeed 97.

New Survey of Electron Impact Cross Sections for Photoelectron and Auroral Electron Energy Loss Calculations

Tariq Majeed and Douglas J. Strickland

Computational Physics, Inc., 2750 Prosperity Avenue, Suite 600, Fairfax, Virginia 22031

Received July 5, 1996; revised manuscript received November 4, 1996

Newly surveyed sets of energy loss cross sections are presented for N_2, O_2, and O. The work was motivated by a number of new electron energy loss measurements in the late 1980s and early 1990s and recent selected review articles. Each set includes a total ionization cross section and excitation cross sections that correspond to all important non-ionizing energy loss channels for that species. A total cross section for each species is constructed by summing the elastic scattering cross section with the ionization and excitation cross sections. The sum is compared to a measured total cross section obtained from electron transmission experiments. Good agreement is achieved for each of the three species. A loss function is also constructed for each species and compared with the Bethe formula above 100 eV. Good agreement is also achieved in energy loss which is dominated by ion and secondary electron production. Fluxes of photoelectrons and auroral electrons have been calculated for the new sets of energy loss cross sections as well as our previous sets. No substantial differences occur using the new description of energy loss.
[S0047-2689(97)00102-5]

Key words: Auroral electron flux; Bethe formula; elastic and total scattering cross sections; electron impact; energy loss cross sections for N_2, O_2 and O; inelastic cross section; ionization cross section; photoelectron flux.

Contents

List of Tables

List of Figures

1. Introduction

The work described below was undertaken as one of several tasks to develop a dayglow/nightglow UV radiance model for the integrated model AURIC (Atmospheric Ultraviolet Radiance Integrated Code). The term *integrated* refers to the joining of this radiance model with the Air Force model MODTRAN. This latter model provides rapid molecular band model calculations of radiances in the IR, transmittances from the IR to the UV, and Rayleigh scattering of sunlight and moonlight.[1–4] The designator AURIC-R will be used to distinguish the UV radiance portion from the integrated model. AURIC-R is being developed by Computational Physics, Inc. (CPI) for the Geophysics Directorate of the Air Force Phillips Laboratory (PL/GP). A key task has been the re-engineering of FORTRAN codes within the PEGFAC (photoelectron g-factor) model[5] using modern programming standards. Another key task has been I/O restructuring and updating of key input parameters. Much of the latter effort has been directed to three sets of electron impact cross sections. These sets are used to 1) perform photoelectron energy loss calculations, 2) calculate volume production rates for chemistry modeling, and 3) calculate volume emission rates for specifying spectral radiances. This paper addresses the first of these sets containing energy loss cross sections for N_2, O_2, and O.

The motivation for this work comes from a number of new cross section measurements in the late 1980s and early 1990s (references to many of these measurements appear in the recent reviews of Itikawa *et al.*,[6,7] Itikawa and Ichimura,[8] Laher and Gilmore,[9] and Kanik *et al.*[10]). Our approach has been to gather cross sections for the important loss channels of each of the three species (a single channel for ionization and several for excitation) and examine them in two ways. First, a total cross section is constructed for each species by summing the total ionization and energy loss cross sections with the elastic scattering cross section for that species. This total cross section is then compared with measurements from electron transmission experiments. Second, a loss function is constructed and compared with the Bethe formula (see Strickland *et al.*[11] for its form and application to N_2) above 100 eV. While such a test is not useful for accurately assessing a cross section set at energies most important to photoelectron energy loss calculations (below 100 eV), it does place constraints on the total inelastic cross section and differential dependence of the ionization cross section above 100 eV. Assuming good knowledge of the total ionization cross section, the differential dependence dictates the magnitudes of the secondary electron energy loss component of the total loss function. This component dominates above a few hundred eV as will be illustrated later in the paper.

Ionization, elastic, and total cross sections of N_2, O_2, and O appear to be well quantified at this time through both laboratory measurements and calculations. As we shall demonstrate, work still remains to be done in quantifying the many excitation (non-ionizing energy loss) channels of these species, especially near and above the first ionization thresh-

old (Rydberg channels). There is generally good agreement among the various sets of total ionization cross section measurements of N_2, O_2, and O (see Itikawa *et al.*,[6,7] Itikawa and Ichimura,[8] and Kanik *et al.*[10] for specific references). The most recent measurements of total ionization cross sections of N_2 (Krishnakumar and Srivastava[12]) and O_2 (Krishnakumar and Srivastava[13]) are in close agreement with earlier measurements of Rapp and Englander-Golden.[14] For O, the recent work by Itikawa and Ichimura[8] lends support to the measurements of Brook *et al.*[15] The total and elastic scattering cross sections of N_2 and O_2 appear to be well characterized based on agreement among the various existing sets of measurements (see the reviews of Itikawa *et al.*[6,7] and Kanik *et al.*[10] for agreement among the original data sets). For O, the only measurement of the total cross section is by Sunshine *et al.*[16] The measurements were limited to energies from 1 to 100 eV and possess more scatter than for the corresponding cross sections of N_2 and O_2. Itikawa and Ichimura[8] constructed a total O cross section by summing available components and found agreement with Sunshine *et al.*[16] within the scatter of the data. The Itikawa and Ichimura[8] cross section spans a larger energy range going to 7000 eV. Within their sum is an elastic scattering cross section based on calculations rather than measurements. The available measurements are by Dehmel *et al.*[17] which appear to be contaminated by inelastic scattering.[8]

Fox and Victor[18] discuss electron energy loss in N_2. Cross section information is in the form of loss function components (for excitation, production of ion states, and kinetic energy of secondaries) with direct cross section information limited to references. Several compiled sets of energy loss cross sections or totals by species have been published over the years in papers addressing the calculation of photoelectron and auroral electron fluxes (e.g., Strickland *et al.*,[11] Victor *et al.*,[19] Oran and Strickland,[20] Jackman and Green,[21] Mantas,[22] Stamnes and Rees,[23] Richards and Torr,[24,25] Solomon,[26] and Strickland *et al.*[27]). The sources of measured and calculated cross sections from one set to another are not the same and in turn can lead to different conclusions from analyses of photoelectron data, auroral electron data, and optical data involving emission features produced by electron impact excitation. A further discussion on this topic will be given in Sec. 5.

Since this paper addresses energy loss cross sections, there will be limited discussion of the collision products associated with a given loss channel. Collision products are important for the other two cross section sets mentioned above, namely for production rates needed in chemistry calculations and emission rates needed in radiance calculations. Energy loss cross sections, on the other hand, are used to calculate photoelectron and auroral electron fluxes for which the only requirement is that a proper distribution of energy loss be achieved per collision. Here, the important features are excitation thresholds, cross section magnitudes, and in the case of ionization, the initial distribution of secondary electrons (for a discussion of the treatment of secondaries in AURIC-R as well as CPI's auroral model, see Strickland *et al.*[11]).

The next three sections present our full sets of energy loss cross sections for N_2, O_2, and O, including references to all individual set members. As noted above, total cross sections are constructed and compared to electron transmission data. Loss functions are also constructed and compared to the Bethe formula. A discussion section (Sec. 5) completes the paper.

2. Energy Loss Cross Sections for N_2

Table 1 identifies states or energy loss channels corresponding to individual inelastic cross sections of N_2. For each entry, the table also includes the energy threshold, location of the cross section maximum, the value of this maximum, the percent contributing to dissociation, and the source of the cross section. Tabulated values of these cross sections (as well as those to follow in Tables 2 and 3) are given in the Appendices. Figure 1 shows examples of measured energy loss spectra (from two separate measurements as noted below) with an energy level diagram above for states with energy thresholds within the illustrated loss region (6 to 14.6 eV). Such data are obtained by starting with a beam of electrons at a single energy and measuring its energy spectrum at a given scattering angle after passing through a given amount of N_2. High lying states from Table 1 are not included since their thresholds (including ionization) lie above 15 eV. Each of the horizontal line segments in the lower portion of the figure is identified with a given state and shows the excitation threshold along with some indication of the effective range of energy loss. Unlike the localized nature of energy loss for an atomic state, here the loss extends to several eV above threshold due to the ability of an impacting electron to leave N_2 in one of several vibrational levels of a given electronic state. The loss spectrum below 12 eV is from S. Trajmar (1995)[71] and was obtained for electrons with an incident energy of 40 eV observed at a scattering angle of 20°. The vertical scale is arbitrary since the purpose of showing the data is to simply illustrate energy loss structure. The wings of the Trajmar loss spectrum have been multiplied by 10 to show the structure associated with the various triplet states. The dominant loss for the given incident energy is seen to be by the $a^1\Pi_g$ state responsible for the Lyman–Birge–Hopfield band system. The loss spectrum above 12 eV is from Ratliff *et al.*[28] for 100 eV electrons scattering through an angle of 15°. The structure above 12.5 eV is dominated by loss to numerous vibrational levels of the b, b′, c, and c′ states. The first figure in Ratliff *et al.*[28] labels the peaks by vibrational level. The magnitude of the Ratliff spectrum is arbitrary and thus no significance is to be placed on its strength relative to the Trajmar spectrum. Cross sections are obtained from data such as these by integrating calibrated spectra over angle and energy loss (see papers such as those of Ratliff *et al.*[28] and Doering and Vaughan[29] for more information on the derivation of cross sections from energy loss data).

Figure 2 shows a comparison between the total cross section based on Table I and transmission measurements taken

TABLE 1. Ionization and excitation cross sections for N_2. We are using these to account for all energy loss to electrons impacting on N_2 in calculations of photoelectron and auroral electron fluxes

Excitation/ ionization	Threshold (eV)	E_{max} (eV)	σ_{max} (10^{-18}) cm^2	% contribution to dissociation	Reference
Total ionization	15.6	100	252	···	12,14
$N_2(X^3\Sigma_g^+)$vib(Total)	0.9	2.0	1540	···	6
$N_2(a^1\Pi_g)$	9.1	18.0	26.9	12	51,59,60,61,72
$N_2(b'^1\Sigma_u^+)$	14.2	60.0	13.6	83	61
$N_2(c_4'^1\Sigma_u)$	12.9	80.0	12.4	15	61
$N_2(b^1\Pi_u)$	12.6	40.0	21.2	96	28,36
$N_2(c^1\Pi_u)$	12.9	40.0	22.0	100	49,36
$N_2(a'^1\Sigma_u^-)$	8.4	15.0	10.4	···	35
$N_2(a''^1\Sigma_g^+)$	12.3	20.0	5.8	···	35
$N_2(w^1\Delta_u)$	8.89	13.0	11.7	···	35
$N_2(A^3\Sigma_u^+)$	6.2	17.0	22.0	···	35
$N_2(B^3\Pi_g)$	7.4	11.5	29.5	···	35
$N_2(C^3\Pi_g)$	11.0	14.0	42.3	50	33,35,61
$N_2(W^3\Delta_u)$	7.5	16.5	38.0	···	35
$N_2(B'^3\Sigma_u^-)$	8.0	15.0	12.5	···	35
$N_2(E^3\Sigma_g^+)$	12.0	24.0	0.8	···	35,36
N_2 (15.8 eV peak)	16.4	40.0	25.0	100	36
N_2 (VUV)	23.7	100	15.5	100	36
N_2 (17.3 eV peak)	17.4	40.0	10.5	100	36
N_2 (N Ryd atoms)	40.0	88.0	3.4	100	36
N_2 (N_2 triplet manifold)	11.0	17.0	13.2	100	36
Other $^1\Pi_u$ states	12.6	40.0	30.0	···	36

from the review by Itikawa *et al.*[6] The total from our work is comprised of the three curves labeled elastic, total ionization, and sum excitation. The elastic cross section was also taken from Itikawa *et al.*[6] The total and elastic cross sections of Itikawa *et al.*[6] are based on available measurements with adjustments to account for offsets among the various data sets. References to original data may be seen in the paper of Itikawa *et al.*[6] (See also Shyn and Carignan,[30] who measured the total elastic cross section from 1.5 to 400 eV. This reference is missing in Itikawa *et al.*[6]). The ionization cross section comes from Rapp and Englander-Golden,[14] which has served as the standard for modeling N_2 ionization in the upper atmosphere. Recent measurements by Krishnakumar and Srivastava[12] are in close agreement with Rapp and Englander-Golden[14] (see also for comparison, the derived total ionization cross section by Shyn[31] from measurements of secondary electrons for primary electron energies from 50 to 400 eV).

The excitation cross section is comprised of the 20 non-ionizing components in Table 1. The next few figures present these components. We start with the triplet state cross sections in Fig. 3. The source of these cross sections is Cartwright *et al.*,[32] except for the C state which is derived from

TABLE 2. Ionization and excitation cross sections for O_2. Similar to Table 1, these are intended to account for all energy loss to electrons impacting on O_2

Excitation/ ionization	Threshold (eV)	E_{max} (eV)	σ_{max} (10^{-18} cm^2)	Reference
Total ionization	12.1	120	297.8	10,13,14
O_2 $(X^3\Sigma_g^+)$ $v=1$	0.3	8.8	35.1	40
O_2 $(X^3\Sigma_g^+)$ $v=2$	0.4	9.9	17.6	40
$O_2(X^3\Sigma_g^+)$ $v=3$	0.6	9.7	7.7	40
O_2 $(X^3\Sigma_g^+)$ $v=4$	0.8	9.3	4.5	40
O_2 $(1^3\Pi_g)$ SR	7.6	18.0	7.0	41
O_2 $(B^3\Sigma_u)$ SR	8.3	19.3	60.6	41
O_2 (8.9 eV peak) SR	8.9	24.3	14.5	41
O_2 (second band) ($^3\Sigma$)	10.3	21.8	1.0	65
O_2 $(a^1\Delta_u)$	1.0	6.0	8.7	63,64
O_2 $(b^1\Sigma_g^+)$	1.6	6.9	3.5	63,64
O_2 (longest band) ($^3\Sigma$)	10.0	24.4	6.8	65
$O_2(A^3\Sigma_u^+ + A'^3\Delta_u + c^1\Sigma_u^-)$	4.5	10.0	17.3	7,64
O_2 (Rydbergs)	16.0	32.0	140.9	20

TABLE 3. Ionization and excitation cross sections for O. Similar to Table 1, these are intended to account for all energy loss to electrons impacting on O

Excitation/ ionization	Threshold (eV)	E_{max} (eV)	σ_{max} (10^{-18}) cm^2	Reference
Total ionization	13.6	100	138	8,15
$2s^2\,2p^4\ ^1D$	2.0	6.0	54.2	47,69
$2s^2\,2p^4\ ^1S$	4.2	11.0	3.36	47,70
$2s^2\,2p^3\,3s\ ^5S^0$	9.3	13.7	3.07	46
$2s^2\,2p^3\,3s^3S^0$	9.5	20.0	11.10	66
$2s^2\,2p^3\,3p\ ^5P$	10.7	16.0	2.5	67
$2s^2\,2p^3\,3p\ ^3P$	11.0	20.0	7.55	67
$2s^2\,2p^3\,3d^3D^0$	12.1	45.6	36.6	66
$2s^2\,2p^3\,3s'\ ^3D$	12.5	49.0	6.43	68
$2s^2\,2p^3\,4d\ ^3D^0$	12.8	45.1	2.0	68
$2s^2\,2p^3\,5d\ ^3D^0$	13.0	50.0	1.13	68
$2s^2\,2p^3\,4d'\ ^3P^0$	16.0	45.1	2.8	68
$2s^2\,2p^5\ ^3P^0$	15.0	45.1	13.2	68
$2s^2\,2p^3\,3s''\ ^3P^0$	14.0	44.8	13.3	68
Rydbergs	14.0	25.0	31.9	20

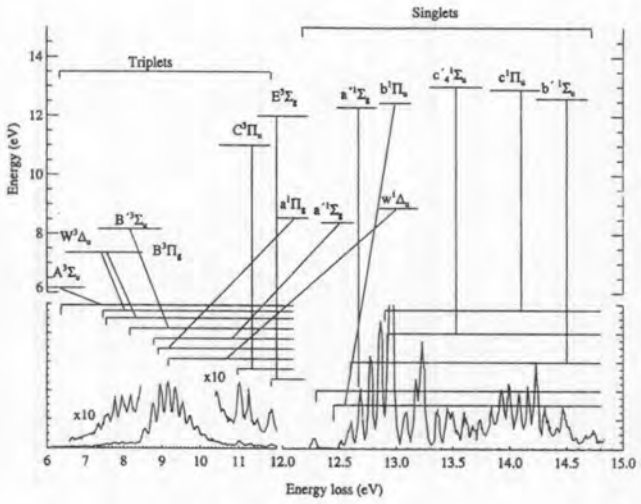

FIG. 1. Measured energy loss spectra for N_2 and energy level diagram showing electronic states contributing to loss in the given energy range. See the text for details on incident electron energies, scattering angles, and references.

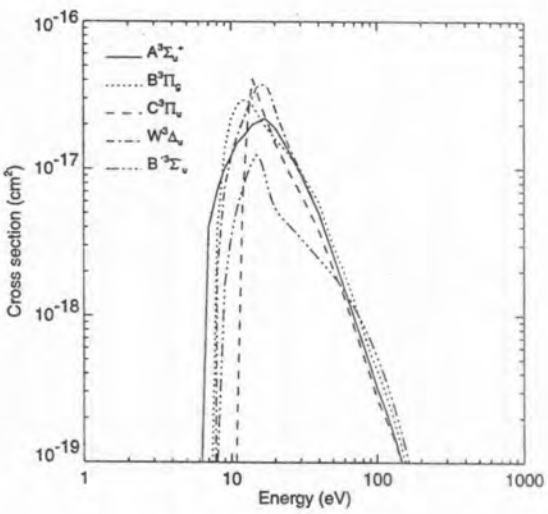

FIG. 3. Excitation cross sections for the identified triplet electronic states of N_2.

Shemansky *et al.*[33] As an added note, Brunger and Teubner[34] have recently performed energy loss measurements similar to Cartwright *et al.*[35] but their results are inconclusive with regard to integrated cross section values due to the restricted range of scattering angles. Singlet state cross sections are shown in Fig. 4 that include the total vibrational cross section and one for high-lying states. Figure 5 shows the terms comprising this latter cross section, which, from Table 1, are seen to come from Zipf and McLaughlin.[36]

In Fig. 6 we show a comparison between the total dissociation cross section that we derive from our full set of cross section data (see Table 1) and those measured by Winters[37] and most recently by Cosby.[38] The cross section data of Winters[37] have been corrected for dissociative ionization by using the recommended values of dissociative ionization cross sections from Itikawa *et al.*[6] Although the values of both measured cross sections for energies greater than 15 eV are within the stated error limits, the systematic differences seen in the figure may be due to an additional error from a correction for dissociative ionization. Our cross section is seen to be in overall good agreement with both measurements.

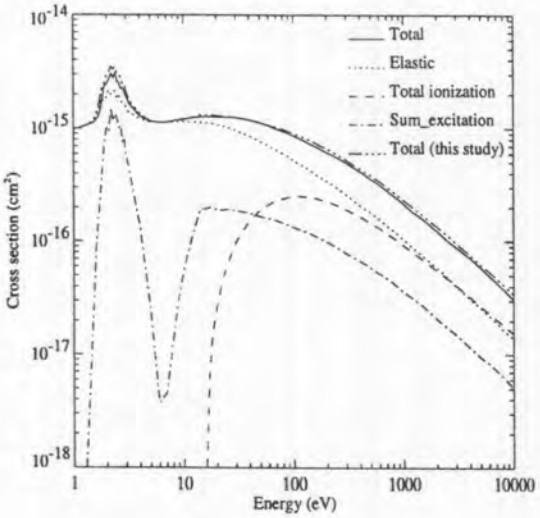

FIG. 2. Comparison between our derived and measured total N_2 cross section. Also shown are the components of our constructed cross section that include elastic, total ionization, and the sum of excitation cross sections from Table 1.

A final figure before discussing O_2 addresses energy loss. The loss function based on Table 1 is compared with the Bethe formula in Fig. 7 (see Strickland *et al.*;[11] Eq. A9 for the form of the Bethe expression). The comparison is restricted to energies above 100 eV since the formula begins to lose its validity at lower energies. The cross section based loss function is calculated from:

$$L(E)=\sum_k W_k\sigma_k(E)+I\sigma_{\text{ioniz}} + \int_0^{(E-I)/2}\frac{d\sigma(E,E_s)}{dE_s}E_s dE_s \quad \text{eV cm}^2. \quad (1)$$

The terms are as follows:

W_k	threshold in eV of the k^{th} excitation process
σ_k	k^{th} excitation cross section
I	average ionization threshold (taken to be 18 eV)
σ_{ioniz}	total ionization cross section
E_s	secondary electron energy
$\frac{d\sigma(E,E_s)}{dE_s}$	differential ionization cross section in eV^{-1} cm^2.

The three components in Eq. 1 are shown in Fig. 7. The importance of the secondary electron component with increasing energy is a reflection of the increase in the average energy of a secondary electron as the energy E of the inci-

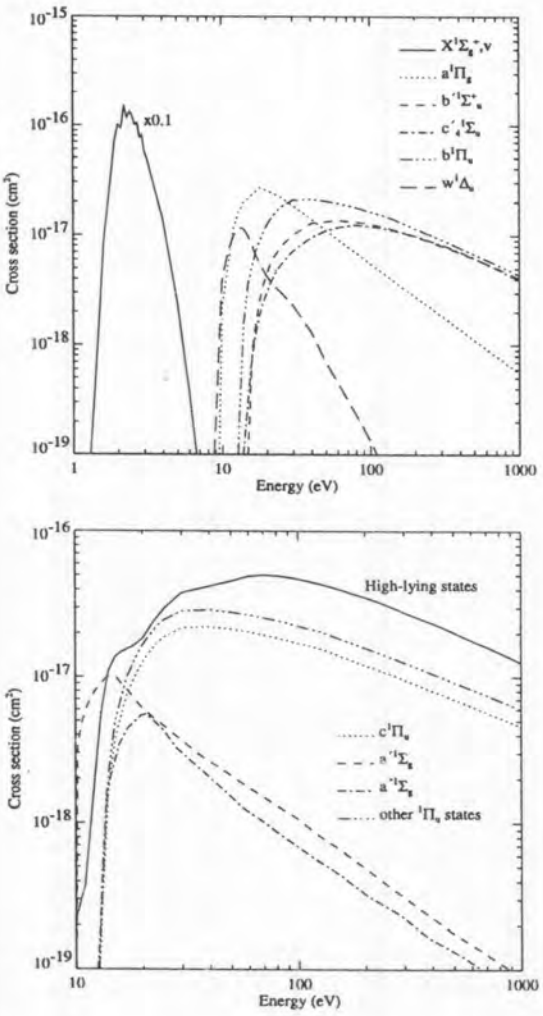

FIG. 4. Excitation cross sections for the identified singlet electronic states of N_2. Vibrational cross sections are summed into a single cross section whose magnitude is reduced by a factor of 10 to be fully displayed in the given panel. Also shown in the lower panel is the sum of the cross sections for the high lying states.

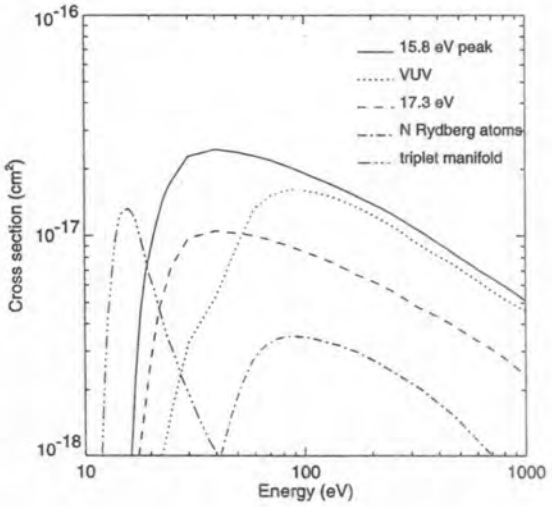

FIG. 5. Individual excitation cross sections for the high lying states.

dent electron increases. The differential form of the ionization cross section is given by Eq. A4 in Strickland *et al.*[11] with the adjustable parameter $\hat{E}=13$ eV. The same value has been used for O_2 and O. Excellent agreement is achieved with the Bethe loss function which gives a strong indication that ionization is being correctly described by its total and differential forms of the cross section. While excitation dominates the loss function below 30 eV, its contribution at higher energies falls below 20% where comparisons with the Bethe loss function become valid. Thus, the test on cross sections using the Bethe formula only weakly addresses excitation.

3. Energy Loss Cross Sections for O_2

Table 2 shows information similar to Table 1 except for O_2. A column has not been included for contributions to dissociation since this is of less interest than for N_2 (this is not to say that the process in not represented within the full set of cross sections presented in the table). Greater interest in N_2 is due to chemistry modeling of N(^4S), N(^2D), N(^2P), and NO within the AURIC model for which production of N in the above states by dissociation (by photoelectrons and solar photons) must be specified. Similar modeling of O is not performed due to O being one of the dominant species in the thermosphere for which its specification is given by a model such as MSISE-90.[39] Like N_2, all excitation cross sections listed in the table are based on energy loss measurements except for those belonging to Rydberg states. Unfortunately, there are no measurements available for these states and consequently we have adopted a theoretical cross section representing total Rydberg excitation as compiled by Oran and Strickland.[20]

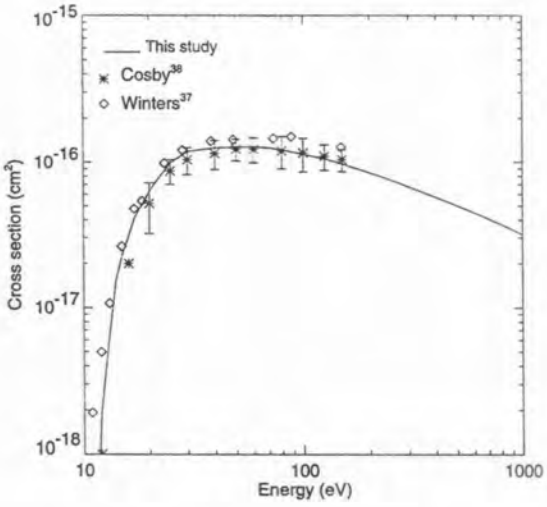

FIG. 6. Derived and measured cross sections for dissociation (excluding dissociative ionization). Error bars refer to the Cosby (Ref. 38) data.

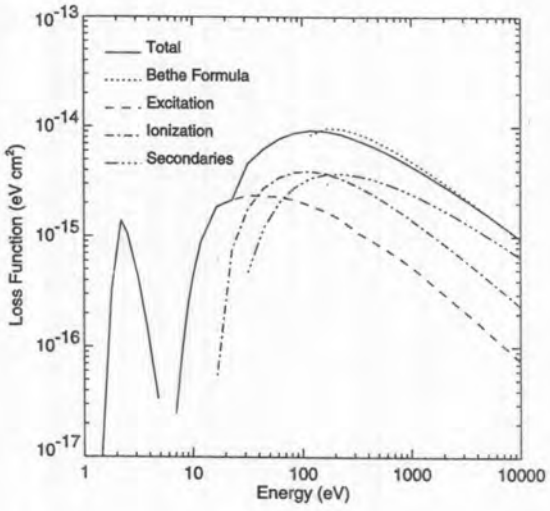

FIG. 7. Loss function from this work compared with the Bethe formula. Also shown are its components from this work.

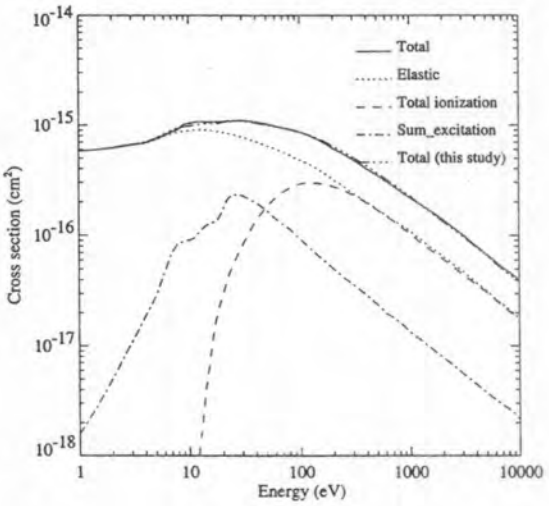

FIG. 9. Total cross section information similar to Fig. 2 except for O_2.

Figure 8 shows O_2 energy loss spectra similar to those for N_2 in Fig. 1. The spectrum below 2 eV is from Shyn and Sweeney[40] for 10 eV electrons scattered through an angle of 96°. The spectrum above 7 eV is from Shyn *et al.*[41] for 20 eV electrons scattered through an angle of 156°. Similar to the spectra for N_2, the results in Fig. 8 have arbitrary scales and thus there is no significance in the strength of the low energy portion compared to that above 7 eV.

Figure 9 shows the measured total cross section, the corresponding cross section based on Table 2, and its three components. The measured total and elastic scattering cross sections come from the most recent review of Kanik *et al.*[10] (see also Sullivan *et al.*,[42] Shyn and Sharp[43] and Wakiya[44] for original studies and other references). Similar to N_2, they are based on several sets of measurements with adjustments for data offsets among these sets. The total ionization cross section also comes from Kanik *et al.*[10] and includes dissociative ionization. These authors compared available measurements and recommend those recently made by Krishnakumar and Srivastava[13] which are similar to the Rapp and Englander-Golden[14] cross section within the stated uncertainty limits. Similar results are also derived by Shyn and Sharp[45] from secondary electron measurements from threshold to 300 eV. The excitation cross section is the sum of the thirteen from Table 2. Figures 10 and 11 show the individual excitation cross sections where a sum has been performed over the vibrational cross sections. Schumann–Runge dissociation is a well known process for O_2. The responsible states are $1^3\Pi_g$ and $B^3\Sigma_g$ along with the 8.9 eV channel listed in Table 2.

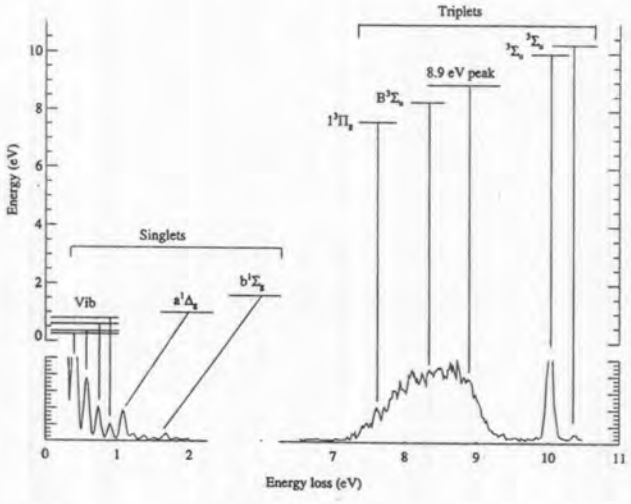

FIG. 8. Examples of energy loss spectra for O_2 and identification of states producing the exhibited structure. See the text for details on incident electron energies, scattering angles, and references.

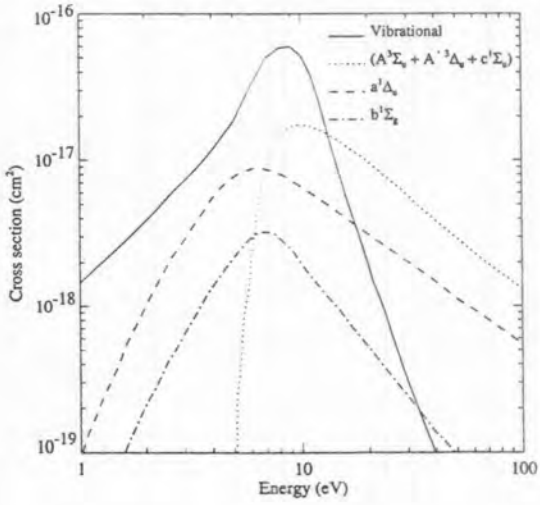

FIG. 10. Cross sections for vibrational excitation (summed over components identified in Table 2), for the singlet states, and for a combined measurement over the $A^3\Sigma_u^+ + A'^3\Delta_u + c'\Sigma_u^-$ states.

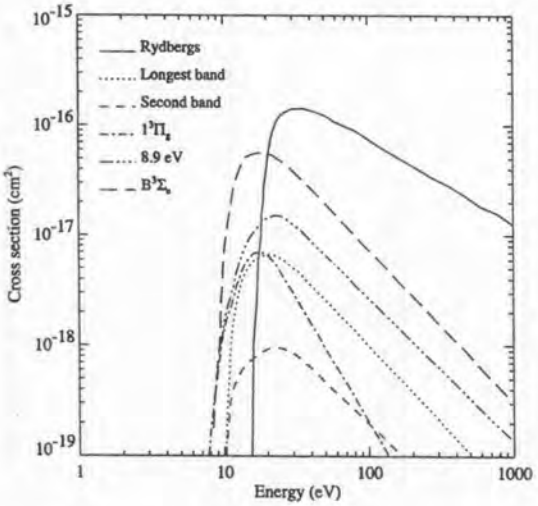

FIG. 11. The remaining excitation cross sections from Table 2.

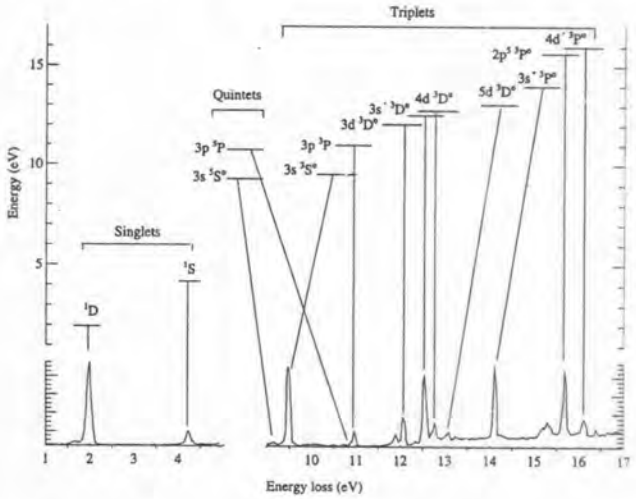

FIG. 13. Examples of energy loss spectra for O and identification of states producing the exhibited structure. See the text for details on incident electron energies, scattering angles, and references.

Figure 12 presents a comparison between the loss function calculated with Eq. 1 and the Bethe loss function. The cross-section-based loss function is about 10% below the Bethe loss function and argues for an increase by this amount in the magnitude of the ionization cross section. As with N_2, energy loss by excitation is minor where the comparison is being made. In fact, excitation plays a weaker role in O_2 compared to N_2. As a concluding comment in this section, larger errors in O_2 energy loss cross sections can be tolerated in photoelectron and auroral electron energy loss calculations compared to N_2 given the fact that there is much less O_2 in the thermosphere.

4. Energy Loss Cross Sections For O

Table 3 shows information for O similar to that in Tables 1 and 2 for N_2 and O_2. There are many high lying states of O in addition to those explicitly listed (see, e.g., Fig. 1 in Laher and Gilmore[9]). None of them individually accounts for significant energy loss based on the measurements of the investigators referenced in the table. The Rydberg cross sections represent these many states not explicitly accounted for. Figure 13 shows energy loss spectra for O similar to previous results in Figs. 1 and 8 for N_2 and O_2, respectively. An important difference, however, is the local nature of energy loss for a given electronic state compared to states of N_2 and O_2 that can extend over several eV due to vibrational excitation. The spectrum below 5 eV is from Doering and Gulcicek[46] for 30 eV electrons scattered through an angle of 120°. The spectrum at higher energies is from Doering and Vanghn[29] for 100 eV electrons scattered through an angle of 4°. Again, as was the case for N_2 and O_2, the scales for the two spectra are arbitrary. We have included energy loss data in Fig. 13 above the ionization threshold (13.6 eV). The slow rise in the underlying continuum above the threshold is due to ionization. The ^5S feature at 9.15 eV has been added based on data from Doering and Gulcicek[47] for 13.9 eV electrons scattered through an angle of 50°. Otherwise, this loss feature would not be discernible given the incident energy (100 eV) associated with rest of the spectrum above 9 eV.

The total cross section for O and its components are shown in Fig. 14. The components are from Itikawa and Ichimura[8] for elastic scattering, Brook *et al.*[15] (see also Itikawa and Ichimura[8]) for ionization, and from the references in Table 3 for excitation. Similar to N_2 and O_2, elastic scattering and ionization dominate the total and thus the comparison in the figure demonstrates little about the accuracy of the total excitation cross section. The next three figures (Figs. 15–17) show the excitation cross sections listed in Table 3. Extrapolations to higher energies beyond those measured are based on expected fall-off for the given transitions.

Similar to O_2, Rydberg cross sections for O are not well

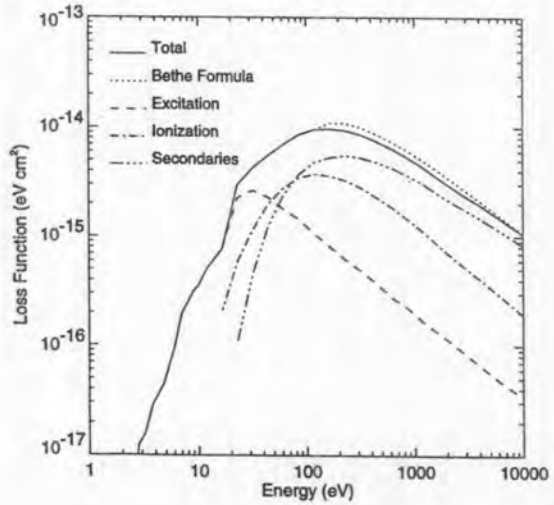

FIG. 12. Loss function information similar to that in Fig. 7 except for O_2.

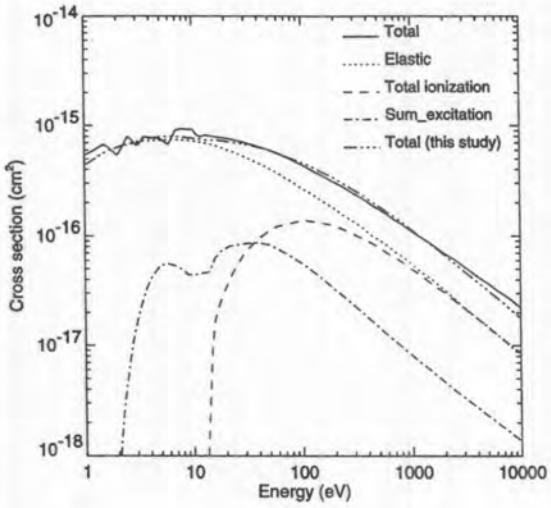

FIG. 14. Total cross section information similar to Fig. 2 except for O.

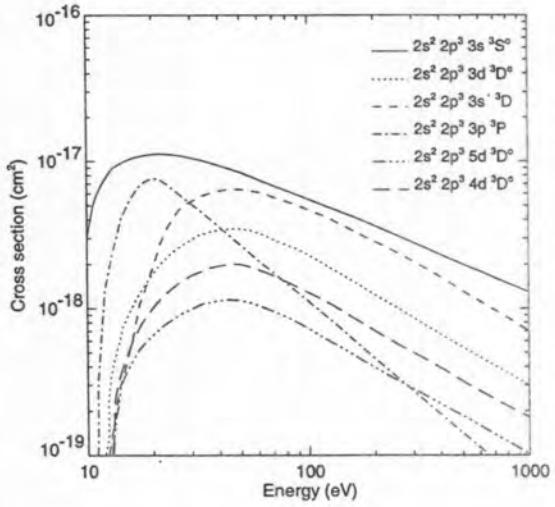

FIG. 16. Cross sections for the triplet states of O.

characterized experimentally, and consequently, we again rely on theoretical values as compiled by Oran and Strickland.[20] The Rydberg cross section in Fig. 15 comes from Oran and Strickland.[20] We are, however, able to compare with other theoretical values produced by Laher and Gilmore[9] who have carried out a critical review of inelastic cross sections for O. They considered more than sixty individual cross sections, including nine allowed and twenty-nine forbidden Rydberg series cross sections with transitions to $O^+(^4S_0)$, $O^+(^2D_0)$, and $O^+(^2P_0)$ ion cores of the excited states. Since no cross section measurements were available, they used a semi-empirical formula based on the work of Jackman *et al.*[48] to estimate individual Rydberg cross sections. Their sum is included in Fig. 15 for comparison with our representation. Good agreement exists below 30 eV while the Laher and Gilmore[9] values are as much as a factor of 2 higher between 40 and 150 eV. There are large uncertainties associated with either cross section and we thus do not speculate as to which is more accurate based on the respective modeling techniques. Nevertheless, using the Laher and Gilmore[9] cross section, our total cross section then exceeds the measured one by about 10% above 30 eV, whereas agreement to within a few percent is achieved using our representation. This provides an argument, although perhaps weak, for implementing a smaller Rydberg cross section above 30 eV than derived from the many individual terms in Laher and Gilmore.[9]

Our calculated loss function for O is shown in Fig. 18 along with that based on the Bethe formula. Reasonably good agreement is achieved with the Bethe formula although the differences in shape and magnitude above several hundred eV suggest increasing the total ionization cross section

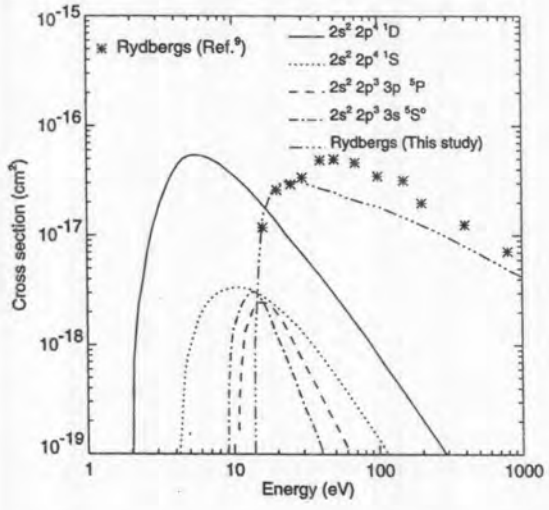

FIG. 15. Cross sections for singlet, quintet and Rydberg states of O. Rydberg cross sections (as summed by us) from Laher and Gimore (Ref. 9) are also shown for comparison.

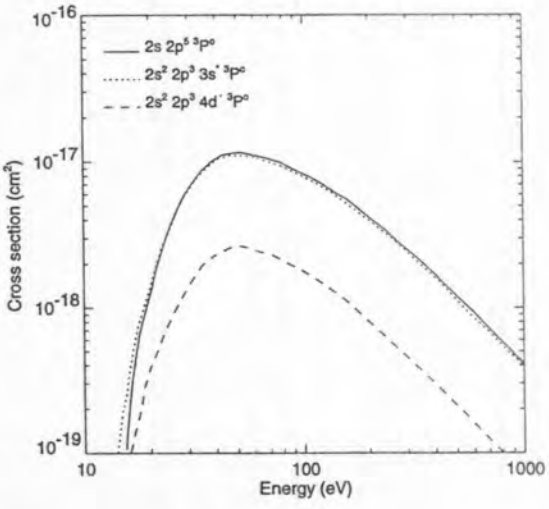

FIG. 17. Autoionization cross sections of O for the following transitions: $^3P \rightarrow 2s\ ^2p^5\ ^3P^0$, $^3P \rightarrow 3s''\ ^3P^0$ and $^3P \rightarrow 4d'\ ^3P^0$.

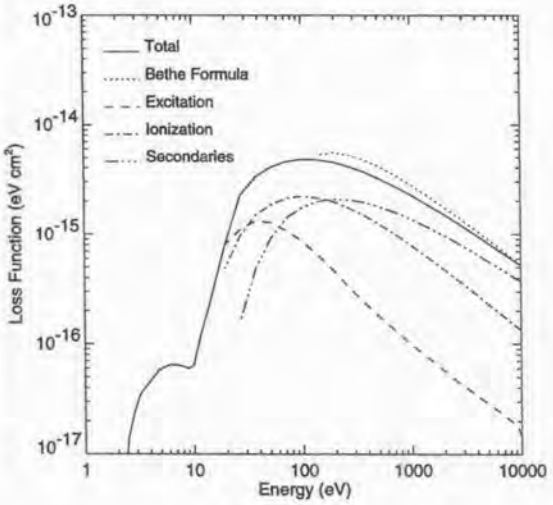

FIG. 18. Loss function information similar to that in Fig. 7 except for O.

by perhaps 20% and decreasing the average energy of the secondary electron per collision by a similar amount.

5. Discussion

From the information presented in earlier sections, it seems clear that there is much less uncertainty in the ionization, elastic, and total cross sections of a particular species compared to excitation. It is difficult to assign error bars due to the many sources of the information although our own assessment is that 15% or less uncertainty can probably be assigned to the former sets and more than 30% should be assigned to the latter (excitation). The largest source of uncertainty for excitation is in the Rydberg cross sections. The situation appears to be most satisfactory for N_2 among the three species being addressed. As noted earlier, we have used calculated values of Rydberg cross sections for O_2 and O given the paucity of measured values. One approach to specifying the total excitation cross section is to 1) subtract the ionization and elastic scattering cross sections from the total cross section or 2) subtract the ionization cross section from the total inelastic cross section (if available). We do not recommend such subtractions since the calculations involve the differences of similar quantities which demand greater accuracy in these quantities than can be expected at this time. An alternative approach and the one taken in this work is to compile available energy loss measurements for specific states or loss channels, supplement them where necessary with theoretical cross sections, sum this total set along with the ionization and elastic scattering cross sections, and compare with the total obtained from transmission measurements. While such an approach does not assure an accurate description for excitation assuming good agreement between totals, it is nevertheless a worthwhile exercise for assigning some degree of confidence to the overall magnitude of the total excitation cross section.

An important aspect of our N_2 work presented in Sec. 2 was specifying a total dissociation cross section. Based on its magnitude (see Fig. 6), dissociation accounts for approximately 80% of the energy loss in excitation channels for electron energies above 30 eV. Given the strength of this loss channel and the importance of odd nitrogen to a number of aeronomical problems, we provide further details here to supplement the discussion in Sec. 2. Zipf and Mclaughlin[36] identified nine energy loss channels that provide most of the contribution to the N_2 dissociation cross section (see Table 1). The most important of these are the high-lying states and the family of $^1\Pi_u$ states (terms used by Zipf and Mclaughlin). Cross section values at 100 eV have recently been measured for two members of this family. Ratliff *et al.*[28] addressed the $b^1\Pi_u$ state and obtained a cross section equal in magnitude to 29% of the value for the family at 100 eV. James *et al.*[49] reported a value for the $c^1\Pi_u$ state equal to 31%. Since these new measurements are available, we have constructed cross sections for these states using the shape of the cross section for the family along with the reported magnitudes at 100 eV. Having removed these components from the Zipf and McLaughlin[36] cross section, a residual cross section for the remaining members was constructed simply by scaling down the Zipf and McLaughlin[36] cross section by 0.40. While the decomposition into three new members with the same shape does not affect photoelectron or auroral electron energy loss calculations, it was done, nevertheless, in anticipation of further measurements of one or more of the $^1\pi_u$ states that may lead to some differences in shapes among the components.

In the Introduction, we noted that several investigators have compiled sets of energy loss cross section for the purpose of calculating photoelectron and auroral electron fluxes and that differences exist among these sets. Generally, there is little difference in ionization and elastic scattering cross sections among the sets. The differences occur among the excitation cross sections. Examples of sets that have noteworthy differences are those of Richards and Torr[24,25] and Strickland and colleagues (e.g., Strickland and Meier;[5] Strickland and Anderson[50]). Specifically, the total N_2 excitation cross section of Richards and Torr[25] is approximately a factor of 2 smaller above 15 eV in comparison to that of Strickland and colleagues. Richards and Torr[25] use a total N_2 excitation cross section obtained by subtracting a total ionization cross section from the total inelastic cross section of Phelps as communicated to Stamnes and Rees[23] (more will be said about this in the next paragraph). Strickland and colleagues have relied heavily on measurements of cross sections for specific states or specific energy loss channels (e.g., Zipf and McLaughlin;[36] Cartwright *et al.*;[32] Ajello and Shemansky[51]). Calculated photoelectron fluxes above 15 eV and below the region where ionization begins to dominate (above about 50 eV) by Richards and Torr[24,25] are approximately twice those of Strickland and colleagues due to these differences. This has led to discussions in numerous papers about the accuracy of the satellite measured photoelectron fluxes by Doering and colleagues (e.g., Lee *et al.*[52]). Rich-

ards and Torr argue that the fluxes have the correct magnitude while Strickland and colleagues argue that the fluxes should be reduced by a factor between 1.5 and 2.0 (e.g., Strickland and Anderson[50]). Conway[53] presents independent information that also argues for a reduction in the measured photoelectron fluxes. A resolution to the problem has not been obtained as of this writing. It is important to note that similar results (within 10%) are obtained by us using either the cross sections in this paper or our earlier sets.

Reference was made in the above paragraph to the total excitation cross section of Phelps in the Stamnes and Rees[23] paper. Phelps (in a private communication to Stamnes and Rees) provided several cross sections for triplet states and one for total excitation to singlet states. Most of the contribution to the total comprising these cross sections comes from an analysis of swarm data. Since investigators such as Stamnes and Rees[23] and Richards and Torr[24] have used cross sections of Phelps and colleagues based on swarm data, a brief discussion of recent papers addressing such data is presented here. The N_2 excitation cross sections appearing in Stamnes and Rees are the same as those published by Pitchford and Phelps[54] with the exception of the total singlet cross section. The version appearing in Stamnes and Rees is about twice as large as in Pitchford and Phelps. The increase is explained by Phelps and Pitchford[55] who added selected high threshold singlet cross sections from Zipf and McLaughlin.[36] Richards and Torr,[25] as noted above, subtracted a total ionization cross section (from Kieffer and Dunn[56]) from the total inelastic cross section in Stamnes and Rees (based on the ionization and excitation cross sections provided by Phelps) to obtain a total excitation cross section. The result is a smaller cross section above the ionization threshold than would be obtained by adding the excitation components of Phelps since the ionization cross section used by Richards and Torr[25] in the subtraction is larger than assumed by Phelps (Rapp and Englander-Golden[14]). In addition to a larger singlet cross section by Phelps and Pitchford[55] compared to their 1982 value, the latter paper also gives a larger total triplet cross section due to an increase in the C state cross section by a factor of 2. The more recent work of Jelenkovic and Phelps,[57] based on stronger electric field swarm data, retains the total singlet cross section from the 1985 work, but returns to a total triplet cross similar to that in the 1982 work. Compared to the compilation in this work, the total singlet cross section is ~25% higher while the total triplet cross section is ~35% smaller.

Although more work remains to be done on characterizing excitation cross sections for N_2, O_2, and O, the compilation from this study gives a comprehensive set of the most updated energy loss cross sections that should serve well for performing photoelectron and auroral electron energy loss calculations. In closing, we note areas that most urgently need more attention:

(1) Measurements of the total scattering cross section of O to verify and understand the limited measurements available at this time. Also needed is an experimental determination of the O elastic scattering cross section.
(2) Measurements to better quantify the Rydberg states of O_2 and O.
(3) Additional selected measurements of the excitation cross sections of the first ten states of N_2 ($A^3\Sigma_u^+$, $B^3\Pi_g$, $W^3\Delta_u$, $C^3\Pi_u$, $B'^3\Sigma_u^-$, $E^3\Sigma_g^+$ triplets and $a'^3\Sigma_u^-$, $a^1\Pi_g$, $w^1\Delta_u$, $a''^1\Sigma_g^+$ singlets) to resolve differences between recent[34] and earlier measurements.[58,32,35])
(4) Measurements of cross sections for various $^1\Pi_u$ states of N_2 to verify the measurement of Zipf and McLaughlin[36] for the sum of cross sections for these states. As noted earlier, single energy measurements have recently been made for the $b^1\Pi_u$ and $c^1\Pi_u$ states. More measurements are needed, especially near 30 eV where these cross sections peak.

6. Acknowledgments

This work was supported under Air Force Phillips Laboratory/Geophysics Directorate Contracts Nos. F19628-92-C-0016 and F19628-95-C-0079. Dr. R. Huffman was the Air Force technical point-of-contact for the work. We thank Dr. R. Link for the use of his tabulations of the following N_2 cross sections: total vibrational, $b'^1\Sigma_u^+$, and $c_4'\,{}^1\Sigma_u$. We would especially like to thank Dr. J. Doering, Dr. S. Trajmar, and Dr. T. W. Shyn for useful discussions. We would also like to thank Dr. J. Doering and Dr. S. Trajmar for reading an earlier version of this paper.

Appendix A. Tabulated Cross Sections for N_2

TABLE 4. Tabulations of the N_2 cross sections for total ionization, total dissociation, and total vibrational excitation

Ionization		Dissociation		Vibrational	
E (eV)	σ (10^{-17} cm^2)	E (eV)	σ (10^{-17} cm^2)	E (eV)	σ (10^{-17} cm^2)
...	...	11	0.070	...	...
...	...	12	0.328	...	...
16	0.113	14	1.77	...	...
18	1.33	16	3.32	1.3	0.111
20	2.68	20	6.59	1.6	8.84
30	9.78	30	12.08	2.0	101.0
50	18.82	50	12.84	2.4	135.0
100	25.20	100	11.43	3.0	58.6
200	22.58	200	8.48	4.0	13.7
500	14.55	500	5.03	5.0	2.34
1000	9.21	1000	3.16	6.0	.366

TABLE 5. Tabulations of the N_2 triplet state cross sections appearing in Fig. 3

$A\ ^3\Sigma_u^+$		$B\ ^3\Pi_g$		$C\ ^3\Pi_g$		$W\ ^3\Delta_u$		$B'\ ^3\Sigma_u^-$	
E (eV)	σ (10^{-17} cm^2)	E (eV)	σ (10^{-17} cm^2)	E (eV)	σ (10^{-17} cm^2)	E (eV)	σ (10^{-17} cm^2)	E (eV)	σ (10^{-17} cm^2)
6.5	0.100	...	...	...	...	...	...	...	...
7.0	0.400	7.6	0.053	...	...	...	...	...	...
8.0	0.700	8.0	0.377	...	...	8.0	0.200	...	...
9.0	1.00	9.0	1.33	...	...	9.0	0.740	9.0	0.160
10	1.23	10	2.19	12	0.58	10	1.20	10	0.350
12	1.65	12	2.93	13	2.53	12	2.10	12	0.740
14	2.00	14	2.70	14	4.23	14	3.06	14	1.13
16	2.13	16	2.16	16	2.70	16	3.73	16	1.14
18	2.10	18	1.84	18	2.07	18	3.50	18	0.730
20	1.90	20	1.60	20	1.73	20	2.57	20	0.540
24	1.40	24	1.31	24	1.21	24	1.57	24	0.430
30	0.919	30	0.973	30	0.77	30	0.972	30	0.337
40	0.500	40	0.592	40	0.40	40	0.500	40	0.245
50	0.262	50	0.304	50	0.25	50	0.262	50	0.190
70	0.096	70	0.125	70	0.12	70	0.096	70	0.114
100	0.032	100	0.042	100	0.069	100	0.032	100	0.053
150	0.009	150	0.012	150	0.31	150	0.010	150	0.015
200	0.004	200	0.003	200	0.002	200	0.004	200	0.004

TABLE 6. Tabulations of the N_2 singlet state cross sections appearing in the upper panel of Fig. 4

$a\ ^1\Pi_g$		$b\ ^1\Pi_u$		$b'\ ^1\Sigma_u^+$		$c_4'\ ^1\Sigma_u$		$w\ ^1\Delta_u$	
E (eV)	σ (10^{-17} cm^2)	E (eV)	σ (10^{-17} cm^2)	E (eV)	σ (10^{-17} cm^2)	E (eV)	σ (10^{-17} cm^2)	E (eV)	σ (10^{-17} cm^2)
...	...	13	0.002	15	0.013	...	...	9	0.018
10	0.220	14	0.157	16	0.089	14	0.012	10	0.362
12	1.15	16	0.526	18	0.256	16	0.081	12	0.981
18	2.69	20	1.21	20	0.436	20	0.298	14	1.15
30	1.86	30	2.08	30	1.01	30	0.719	16	0.806
50	1.12	50	2.04	50	1.32	50	1.10	20	0.430
100	0.559	100	1.63	100	1.26	100	1.20	30	0.231
200	0.280	200	1.16	200	0.978	200	0.995	50	0.071
500	0.111	500	0.676	500	0.623	500	0.629	100	0.013
1000	0.056	1000	0.440	1000	0.409	1000	0.394	200	0.001

TABLE 7. Tabulations of the N_2 singlet state cross sections appearing in the lower panel of Fig. 4

$c\ ^1\Pi_u$		$a'\ ^1\Sigma_u^-$		$a''\ ^1\Sigma_g^+$		Other $^1\Pi_u$ states	
E (eV)	σ (10^{-17} cm^2)	E (eV)	σ (10^{-17} cm^2)	E (eV)	σ (10^{-17} cm^2)	E (eV)	σ (10^{-17} cm^2)
...	...	11	0.48	13	0.035	...	...
13	0.002	12	0.652	14	0.182	13	0.002
14	0.163	14	0.950	16	0.368	14	0.216
16	0.549	16	0.850	20	0.551	16	0.724
20	1.26	20	0.480	25	0.426	20	1.66
30	2.17	30	0.230	30	0.304	30	2.86
50	2.13	50	0.193	50	0.152	50	2.81
100	1.70	100	0.096	100	0.069	100	2.25
200	1.21	200	0.045	200	0.033	200	1.59
500	0.705	500	0.016	500	0.013	500	0.930
1000	0.458	1000	0.008	1000	0.007	1000	0.605

TABLE 8. Tabulations of the N_2 high lying state cross sections appearing in Fig. 5

15.8 eV peak		VUV		17.3 eV peak		N Rydberg atoms		Triplet manifold	
E (eV)	σ (10^{-17} cm^2)	E (eV)	σ (10^{-17} cm^2)	E (eV)	σ (10^{-17} cm^2)	E (eV)	σ (10^{-17} cm^2)	E (eV)	σ (10^{-17} cm^2)
...	...	...	...	...	...	...	...	12	0.123
...	...	...	...	...	...	...	...	13	0.519
17	0.225	...	...	...	...	...	...	14	1.03
18	0.453	25	0.161	18	0.120	...	...	16	1.31
20	0.852	30	0.328	20	0.270	...	...	18	0.986
25	1.74	40	0.529	25	0.720	...	...	20	0.645
30	2.28	50	0.897	30	0.970	50	0.186	25	0.313
50	2.39	70	1.51	50	1.02	70	0.327	30	0.192
100	1.92	100	1.60	100	0.850	100	0.348	40	0.103
200	1.40	200	1.24	200	0.626	200	0.275	50	0.066
500	0.800	500	0.712	500	0.377	500	0.144	70	0.027
1000	0.510	1000	0.456	1000	0.232	1000	0.061	1000	0.007

Appendix B. Tabulated Cross Sections for O_2

TABLE 9. Tabulations of the O_2 cross sections for total vibrational excitation, Rydbergs, and total ionization

Vibrational		Rydbergs		Ionization	
E (eV)	σ (10^{-17} cm^2)	E (eV)	σ (10^{-17} cm^2)	E (eV)	σ (10^{-17} cm^2)
1	0.145	...	...	...	...
2	0.381	...	...	13	0.200
3	0.720	17	0.281	16	1.09
4	1.17	20	4.18	20	2.93
6	3.24	30	14.09	30	8.08
9	5.98	50	12.36	50	18.24
12	2.59	100	7.59	100	29.08
15	0.755	200	4.34	200	27.46
20	0.191	500	2.18	500	17.10
30	0.030	1000	1.26	1000	10.54

TABLE 10. Tabulations of the O_2 electronic state cross sections appearing in Fig. 10

A+A'+c		$a^1\Delta_u$		$b\ ^1\Sigma_g^+$	
E (eV)	σ (10^{-17} cm^2)	E (eV)	σ (10^{-17} cm^2)	E (eV)	σ (10^{-17} cm^2)
6	0.211	...	...	...	...
7	0.846	2	0.098	2	0.021
8	1.41	3	0.283	3	0.064
10	1.73	4	0.548	5	0.214
15	1.33	6	0.870	7	0.324
20	0.974	10	0.661	9	0.247
30	0.580	20	0.316	13	0.117
50	0.297	50	0.113	20	0.052
100	0.131	100	0.055	30	0.024
150	0.088	150	0.035	50	0.009
200	0.068	200	0.025	100	0.002

TABLE 11. Tabulations of the O_2 cross sections appearing in Fig. 11 excluding the Rydberg cross section (see Table 9)

Longest band		Second band		$1\ ^3\Pi_g$		8.9 eV		$B\ ^3\Sigma_u$	
E (eV)	σ (10^{-17} cm^2)	E (eV)	σ (10^{-17} cm^2)	E (eV)	σ (10^{-17} cm^2)	E (eV)	σ (10^{-17} cm^2)	E (eV)	σ (10^{-17} cm^2)
...	...	...	...	...	...	9	0.058	...	...
...	...	...	...	8	0.017	10	0.162	9	0.075
11	0.083	...	...	9	0.059	12	0.413	10	0.639
12	0.212	12	0.046	10	0.137	15	0.918	12	2.98
15	0.519	15	0.071	11	0.210	20	1.42	15	5.29
20	0.670	20	0.093	13	0.431	25	1.49	20	5.58
30	0.510	30	0.086	18	0.700	30	1.27	30	3.91
50	0.264	50	0.047	24	0.502	50	0.671	50	1.99
100	0.100	100	0.020	30	0.307	100	0.271	100	0.748
200	0.038	200	0.008	50	0.095	200	0.109	200	0.285
500	0.011	500	0.001	100	0.021	500	0.034	500	0.082
1000	0.002	...	...	200	0.003	1000	0.014	1000	0.030

Appendix C. Tabulated Cross Sections for O

TABLE 12. Tabulations of the O cross sections appearing in Fig. 15 plus the total ionization cross section

^1D		^1S		^5P		^5S		Ionization		Rydbergs	
E (eV)	σ (10^{-17} cm^2)	E (eV)	σ (10^{-17} cm^2)	E (eV)	σ (10^{-17} cm^2)	E (eV)	σ (10^{-17} cm^2)	E (eV)	σ (10^{-17} cm^2)	E (eV)	σ (10^{-17} cm^2)
2.3	0.274	...	...	...	...	9.5	0.077	...	...	15	0.556
3	1.55	4.5	0.032	...	...	10	0.140	...	...	16	1.53
4	3.95	5	0.090	11	0.040	11	0.205	14	0.230	18	2.34
5.5	5.41	6	0.190	12	0.134	12	0.261	16	1.72	20	2.85
8	4.59	8	0.302	14	0.223	14	0.307	20	3.30	25	3.19
10	3.61	11	0.336	16	0.246	17	0.210	30	7.06	30	3.14
15	2.10	15	0.293	20	0.194	20	0.119	50	11.06	50	2.58
20	1.33	20	0.223	25	0.115	25	0.058	100	13.80	100	1.90
30	0.681	30	0.131	30	0.070	30	0.029	200	12.22	200	1.28
50	0.290	50	0.053	50	0.019	50	0.004	500	7.92	500	0.712
100	0.081	100	0.014	100	0.002	100	...	1000	4.99	1000	0.436

TABLE 13. Tabulations of the O cross sections appearing in Fig. 16

$3s^3S$		$3d^3D$		$3s'^3D$		$3p^3P$		$5d^3D$		$4d^3D$	
E (eV)	σ (10^{-17} cm^2)	E (eV)	σ (10^{-17} cm^2)	E (eV)	σ (10^{-17} cm^2)	E (eV)	σ (10^{-17} cm^2)	E (eV)	σ (10^{-17} cm^2)	E (eV)	σ (10^{-17} cm^2)
...	...	...	...	13	0.014	...	...	...	...	...	...
...	...	12	0.010	14	0.028	12	0.120	...	...	...	...
10	0.302	13	0.037	16	0.057	14	0.344	...	...	13	0.015
12	0.732	14	0.057	18	0.120	16	0.555	14	0.024	14	0.033
15	0.998	16	0.091	20	0.187	20	0.755	16	0.043	16	0.057
20	1.11	20	0.170	25	0.415	25	0.641	20	0.065	20	0.100
30	1.05	30	0.293	30	0.532	30	0.517	30	0.100	30	0.168
50	0.836	50	0.347	50	0.642	50	0.275	50	0.113	50	0.199
100	0.557	100	0.232	100	0.470	100	0.114	100	0.073	100	0.128
200	0.369	200	0.125	200	0.288	200	0.050	200	0.040	200	0.071
500	0.206	500	0.055	500	0.133	500	0.014	500	0.020	500	0.032
1000	0.131	1000	0.030	1000	0.070	...	...	1000	0.010	1000	0.018

TABLE 14. Tabulations of the O cross sections appearing in Fig. 17

$2p^5\ ^3P$		$3s''\ ^3P$		$4d'\ ^3P$	
E (eV)	σ (10^{-17} cm^2)	E (eV)	σ (10^{-17} cm^2)	E (eV)	σ (10^{-17} cm^2)
16	0.020	16	0.035	...	...
18	0.069	18	0.084	18	0.019
20	0.123	20	0.137	20	0.038
25	0.371	25	0.360	25	0.085
30	0.648	30	0.632	30	0.140
50	1.15	50	1.10	50	0.264
100	0.828	100	0.794	100	0.178
200	0.420	200	0.400	200	0.081
500	0.120	500	0.114	500	0.021
1000	0.041	1000	0.039	800	0.010

7. References

[1] F. X. Kneizys, E. P. Shettle, L. W. Abreu, J. H. Chetwynd, G. P. Anderson, W. O. Gallery, J. E. A. Selby, and S. A. Clough, AFGL Technical Report No. AFGL-TR-88-0177, Air Force Phillips Lab., Hanscom AFB, MA (1988).

[2] A. Berk, L. Bernstein, and D. Robertson, AFGL Technical Report No. AFGL-TR-89-0122, Air Force Phillips Lab., Hanscom AFB, MA (1989).

[3] G. P. Anderson, J. H. Chetwynd, J.-M. Therault, P. Acharya, A. Berk, D. C. Robertson, F. X. Kneizys, M. L. Hohe, L. W. Abreu, and E. P. Shettle, Proc. SPIE Int. Soc. Opt. Eng. **1968**, 514 (1993).

[4] K. Minschwaner, G. P. Anderson, L. A. Hall, J. H. Chetwynd, R. J. Thomas, D. W. Rusch, A. Berk, and J. A. Conant, J. Geophys. Res. **100**, 11,165 (1995).

[5] D. J. Strickland and R. R. Meier, NRL Memorandum Report No. 5004 (1982).

[6] Y. Itikawa, M. Hayashi, A. Ichimura, K. Onda, K. Sakimoto, K. Takayanagi, M. Nakamura, H. Nishimura, and T. Takayanagi, J. Phys. Chem. Ref. Data **15**, 985 (1986).

[7] Y. Itikawa, A. Ichimura, K. Onda, K. Sakimoto, K Takayanagi, Y. Hatano, M. Hayashi, H. Nishimura, and S. Tsurubuchi, J. Phys. Chem. Ref. Data **18**, 23 (1989).

[8] Y. Itikawa and A. Ichimura, J. Phys. Chem. Ref. Data **19**, 637 (1990).

[9] R. R. Laher and F. R. Gilmore, J. Phys. Chem. Ref. Data **19**, 277 (1990).

[10] I. S. Kanik, S. Trajmar, and J. C. Nickel, J. Geophys. Res. **98**, 7447 (1993).

[11] D. J. Strickland, D. L. Book, T. P. Coffey, and J. A. Fedder, J. Geophys. Res. **81**, 2755 (1976).

[12] E. Krishnakumar and S. K. Srivastava, J. Phys. B **23**, 1893 (1990).

[13] E. Krishnakumar and S. K. Srivastava, Int. J. Mass Spectrom. Ion Processes **113**, 1 (1992).

[14] D. Rapp and P. Englander-Golden, J. Chem. Phys. **43**, 1464 (1965).

[15] E. M. Brook, F. A. Harrison, and A. C. Smith, J. Phys. B **11**, 3115 (1978).

[16] G. Sunshine, B. B. Aubrey, and B. Berderson, Phys. Rev. **154**, 1 (1967).

[17] R. C. Dehmel, M. A. Fineman, and D. R. Miller, Phys. Rev. A **13**, 115 (1976).

[18] J. L. Fox and G. A. Victor, Planet. Space Sci. **36**, 329 (1988).

[19] G. Victor, K. Kirby-Docken, and A. Dalgarno, Planet. Space Sci. **24**, 679 (1976).

[20] E. S. Oran and D. J. Strickland, Planet. Space Sci. **26**, 1161 (1978).

[21] C. H. Jackman and A. E. S. Green, J. Geophys. Res. **84**, 2715 (1979).

[22] G. P. Mantas, Planet. Space Sci. **29**, 1319 (1981).

[23] K. Stamnes and M. H. Rees, J. Geophys. Res. **88**, 6301 (1983).

[24] P. G. Richards and D. G. Torr, J. Geophys. Res. **93**, 4060 (1988).

[25] P. G. Richards and D. G. Torr, J. Geophys. Res. **89**, 5625 (1984).

[26] S. C. Solomon, P. Hays, and V. J. Abreu, J. Geophys. Res. **93**, 9867 (1988).

[27] D. J. Strickland, R. R. Meier, J. H. Hecht, and A. B. Christensen, J. Geophys. Res. **94**, 13527 (1989).

[28] J. M. Ratliff, G. K. James, S. Trajmar, J. M. Ajello, and D. E. Shemansky, J. Geophys. Res. **96**, 17559 (1991).

[29] J. P. Doering and S. O. Vaughan, J. Geophys. Res. **91**, 3279 (1986).

[30] T. W. Shyn and G. R. Carignan, Phys. Rev. A **22**, 923 (1980).

[31] T. W. Shyn, Phys. Rev. A **27**, 2388 (1983).

[32] D. C. Cartwright, S. Trajmar, A. Chutjian, and W. Williams, Phys. Rev. A **16**, 1013 (1977).

[33] D. E. Shemansky, J. M. Ajello, and I. Kanik, Astrophys. J. **452**, 472 (1995).

[34] M. J. Brunger and P. J. O. Teubner, Phys. Rev. A **41**, 1413 (1990).

[35] D. C. Cartwright, S. Trajmar, A. Chutjian, and W. Williams, Phys. Rev. A **16**, 1041 (1977).

[36] E. C. Zipf and R. W. McLaughlin, Planet. Space Sci. **26**, 449 (1978).

[37] H. J. Winters, J. Chem. Phys. **44**, 1472 (1966).

[38] P. C. Cosby, J. Chem. Phys. **98**, 9544 (1993).

[39] A. E. Hedin, J. Geophys. Res. **96**, 1159 (1991).

[40] T. W. Shyn and C. J. Sweeney, Phys. Rev. A **48**, 1214 (1993).

[41] T. W. Shyn, C. J. Sweeney, A. Grafe, and W. E. Sharp, Phys. Rev. A **50**, 4794 (1994).

[42] J. P. Sullivan, J. C. Gibson, R. J. Gulley, and S. J. Buckman, J. Phys. B **28**, 4319 (1995).

[43] T. W. Shyn and W. E. Sharp, Phys. Rev. A **26**, 1369 (1982).

[44] K. Wakiya, J. Phys. B **11**, 3913 (1978).

[45] T. W. Shyn and W. E. Sharp, Phys. Rev. A **43**, 2300 (1991).

[46] J. P. Doering and E. E. Gulcicek, J. Geophys. Res. **94**, 2733 (1989).

[47] J. P. Doering and E. E. Gulcicek, J. Geophys. Res. **94**, 1541 (1989).

[48] C. H. Jackman, R. M. Garvey, and A. E. S. Green, J. Geophys. Res. **82**, 5081 (1977).

[49] G. K. James, J. M. Ajello, B. Franklin, and D. E. Shemansky, J. Phys. **23**, 2055 (1990).

[50] D. J. Strickland and D. E. Anderson, J. Geophys. Res. **88**, 9260 (1983).

[51] J. M. Ajello and D. E. Shemansky, J. Geophys. Res. **90**, 9845 (1985).

[52] J. S. Lee, J. P. Doering, T. A. Potemra, and L. H. Brace, Planet. Space Sci. **28**, 947 (1980).

[53] R. R. Conway, Planet. Space Sci. **31**, 1223 (1983).

[54] L. C. Pitchford and A. V. Phelps, Phys. Rev. A **25**, 540 (1982).

[55] A. V. Phelps and L. C. Pitchford, Phys. Rev. A **31**, 2932 (1985).

[56] L. J. Kieffer and G. H. Dunn, Rev. Mod. Phys. **38**, 1 (1966).

[57] B. M. Jelenkovic and A. V. Phelps, Phys. Rev. A **36**, 5310 (1987).

[58] S. Trajmar, D. F. Register, and A. Chutjian, Phys. Rep. **97**, 219 (1983).

[59] K. D. Pang, J. M. Ajello, B. Franklin, and D. E. Shemansky, J. Chem. Phys. **86**, 2750 (1987).

[60] N. J. Mason and W. R. Newell, J. Phys. B **20**, 3913 (1987).

[61] J. M. Ajello, G. K. James, B. O. Franklin, and D. E. Shemansky, Phys. Rev. A **40**, 3524 (1989).

[62] R. R. Meier, Space Sci. Rev. **58**, 1 (1991).

[63] T. W. Shyn and C. J. Sweeney, Phys. Rev. A **47**, 1006 (1993).

[64] K. Wakiya, J. Phys. B **11**, 3931 (1978).

[65] T. W. Shyn, C. J. Sweeney, and A. Grafe, Phys. Rev. A **49**, 3680 (1994).

[66] E. E. Gulcicek and J. P. Doering, J. Geophys. Res. **93**, 5879 (1988).

[67] E. E. Gulcicek, J. P. Doering, and S. O. Vaughan, J. Geophys. Res. **93**, 5885 (1988).

[68] S. O. Vaughan and J. P. Doering, J. Geophys. Res. **93**, 289 (1988).

[69] T. W. Shyn, J. Geophys. Res. **91**, 1691 (1986).

[70] T. W. Shyn, S. Y. Cho, and W. E. Sharp, J. Geophys. Res. **91**, 13751 (1986).

[71] S. Trajmar (private communication).

[72] D. J. Strickland, T. Majeed, J. S. Evans, R. R. Meier, and J. M. Picone, J. Geophys. Res. (submitted, 1997).